Fischer-Tropsch synthesis: study of the promotion of Pt on the reduction property of Co/Al_2O_3 catalysts by *in situ* EXAFS of Co *K* and Pt L_{III} edges and XPS

Gary Jacobs,[a] John A. Chaney,[b] Patricia M. Patterson,[b] Tapan K. Das,[b] Julie C. Maillot[b] and Burtron H. Davis[b]*

[a]University of Louisville, Department of Chemical Engineering, Louisville, KY 40292, USA, and [b]Center for Applied Energy Research, 2540 Research Park Drive, Lexington, KY 40511, USA. E-mail: davis@caer.uky.edu

The addition of platinum metal to cobalt/alumina-based Fischer-Tropsch synthesis (FTS) catalysts increases both the reduction rate and, consequently, the density of active cobalt sites. Platinum also lowers the temperature of the two-step conversion of cobalt oxide to cobalt metal observed in temperature programmed reduction (TPR) as Co_3O_4 to CoO and CoO to Co^0. The interaction of the alumina support with cobalt oxide ultimately determines the active site density of the catalyst surface. This interaction can be controlled by varying the cobalt loading and dispersion, selecting supports with differing surface areas or pore sizes, or changing the noble metal promoter. However, the active site density is observed to depend primarily on the cluster size and extent of reduction, and there is a direct relationship between site density and FTS rate. In this work, *in situ* extended X-ray absorption fine structure (EXAFS) at the L_{III} edge of Pt was used to show that isolated Pt atoms interact with supported cobalt clusters without forming observable Pt—Pt bonds. *K*-edge EXAFS was also used to verify that the cobalt cluster size increases slightly for those systems with Pt promotion. X-ray absorption near-edge spectroscopy (XANES) was used to examine the remaining cobalt clusters after the first stage of TPR, and it revealed that the species were almost entirely cobalt (II) oxide. After the second stage of TPR to form cobalt metal, a residual oxide persists in the sample, and this oxide has been identified as cobalt (II) aluminate using X-ray photoelectron spectroscopy (XPS). Sequential *in situ* reduction of promoted and unpromoted systems was also monitored through XPS, and Pt was seen to increase the extent of cobalt reduction by a factor of two.

Keywords: cobalt; alumina; Fischer-Tropsch; reducibility; EXAFS; XPS.

1. Introduction

Cobalt-based Fischer-Tropsch synthesis (FTS) catalysts show promise for gas-to-liquid (GTL) conversion owing to their low water–gas shift activity (Espinoza *et al.*, 1998; van Berge *et al.*, 2001). Commercial FTS catalysts contain high loadings of cobalt to offset adverse reoxidation phenomena. Such loadings are often as high as 30 g Co/100 g Al_2O_3 (Espinoza *et al.*, 1998; van Berge *et al.*, 2001). Even at these high loadings a significant fraction of cobalt is left in an unreduced state after a standard activation procedure (*e.g.* 1 atm H_2 at 623 K for 10 h) (van de Loosdrecht *et al.*, 2000; Arnoldy & Moulijn, 1985; Moen & Nicholson, 1997; Lapidus *et al.*, 1991; Wang & Chen, 1991; Jongsomjit *et al.*, 2001; Hilmen *et al.*, 1999; Voss *et al.*, 2002; Enache *et al.*, 2002; Bechara *et al.*, 2002; Jacobs, Das *et al.*, 2002). Noble metal promoters such as Ru, Pt and Re (Arnoldy & Moulijn, 1985; Jacobs, Das *et al.*, 2002; Ronning *et al.*, 2001; Guczi *et al.*, 2002; Kogelbauer *et al.*, 1996; Hilmen *et al.*, 1996; Schanke *et al.*, 1995; Vada *et al.*, 1995; Rygh & Nielsen, 2000; Tang *et al.*, 1999) are often employed to facilitate the reduction of cobalt oxide species interacting with the support, thereby generating more active surface sites for catalysis.

The nature of the interaction and operation of cobalt species on the alumina support remain controversial. It is known that Co/Al_2O_3 exhibits a temperature programmed reduction (TPR) profile with two major peaks similar to bulk cobalt and Co/SiO_2. For bulk cobalt and 15%Co/SiO_2 catalysts, one TPR peak is situated near 548 K and a much larger peak (about three times the area) is situated near 613 K. The two prominent TPR peaks have been assigned to a two-step reduction of the metal oxide from Co_3O_4 to CoO and then CoO to Co^0. A small third peak above 1073 K has been assigned to the reduction of cobalt aluminate (Wang & Chen, 1991). In the case of Co/Al_2O_3 the two peaks are significantly broadened, with the second extending up to temperatures of 1003 K (Moulijn, 1985; Jongsomjit *et al.*, 2001; Hilmen *et al.*, 1996, 1999; Ronning *et al.*, 2001; Kogelbauer *et al.*, 1996; Schanke *et al.*, 1995; Vada *et al.*, 1995). Another explanation suggests that the first step, Co_3O_4 to CoO, is kinetically fast giving rise to a sharp lower-temperature peak, but subsequent reduction of CoO depends on cluster size with the smaller clusters being rate limiting owing to the support interaction (Lapidus *et al.*, 1991; Wang & Chen, 1991; Sexton *et al.*, 1986). While the reduction of Co_3O_4 was found to be fast regardless of cluster size, the reduction sensitivity of CoO to cluster size has indeed been supported (Bart, 1986; Castner *et al.*, 1983).

Small amounts of noble metal are commonly added to cobalt oxides to promote the reduction of cobalt and enhance syngas (*i.e.* CO and H_2) conversion. We have previously reported on the nature of the rhenium interaction with supported cobalt oxide FTS systems (Jacobs *et al.*, 2004), and now we expand upon this earlier discussion to include the chemistry of the platinum interaction with cobalt oxide. Recent work using extended X-ray absorption fine structure (EXAFS) suggests that an intimate association of Pt with Co is required to promote reduction (Guczi *et al.*, 2002). In that study no Pt—Pt coordination was found in the Fourier transform at a coordination distance of 2.7 Å, but a significant peak was observed at 2.2 Å which the authors ascribed to a Pt—Co bond distance (Guczi *et al.*, 2002). It is suggested that Pt is likely to be situated on the edge of the cluster, and it is further suggested that reduction occurs on Pt first, allowing hydrogen to spill over to the cobalt oxide and nucleate cobalt metal sites. This scenario is supported by TPR, and a comparison of various noble metals showed that reduction of the promoter is first required to achieve the promoting effect. As pointed out in our previous TPR work (Jacobs, Das *et al.*, 2002), the degree of reduction *versus* temperature strongly suggests a nucleation and growth mechanism for the reduction process. That is, once cobalt metal nuclei are available for the dissociation of hydrogen (*i.e.* the slow step), the reduction proceeds at a rapid rate. In fact, significant shifts to lower temperature in cobalt oxide reduction have been observed with Pt and Ru addition (Jacobs, Das *et al.*, 2002; Guczi *et al.*, 2002; Kogelbauer *et al.*, 1996; Schanke *et al.*, 1995). However, in the case of Re only the second reduction step is significantly affected (Hilmen *et al.*, 1996, 1999; Jacobs, Das *et al.*, 2002), owing to the reduction of Re occurring near the same temperature as the first stage of Co_3O_4 to CoO.

It is also important to understand how the average cluster size is affected by Pt addition. For similar reduction temperatures, Pt has the benefit of assisting the reduction of those cobalt oxide species which have strong interactions with the alumina support. These cobalt oxide

  DOI: 10.1107/S090904950401578X

clusters are likely to be small in size, and they may remain independent on the surface or combine with larger clusters. Previously we have reported on the interaction of Re with supported cobalt oxide clusters for FTS (Jacobs *et al.*, 2004). In this study we expand upon the earlier discussion by evaluating the platinum interaction using a similar methodology as before. We will examine the oxidation state changes of cobalt with hydrogen exposure by evaluating data from X-ray photoelectron (XPS) and X-ray absorption near-edge (XANES) spectroscopies. The spectral information will be related to oxidation state and cluster size changes with the aid of TPR and EXAFS. The electronic state and local structure of the Pt promoter will also be examined.

2. Experimental

2.1. Catalyst preparation

2.1.1. 15%Co/Al_2O_3 catalyst. Condea Vista Catalox (high-purity γ-alumina, 200 $m^2\ g^{-1}$) was used as the support. The catalyst was prepared by incipient wetness impregnation (IWI) and cobalt nitrate was used as the precursor. To obtain a cobalt loading of 15%, a three-step impregnation was used with drying at 353 K in a rotary evaporator following each impregnation. After the final impregnation/drying step, the catalyst was calcined under air flow at 673 K for 4 h. For the platinum-promoted catalyst, the salt used was tetraamine platinum (II) nitrate and it was added by IWI after the last drying step associated with cobalt addition, but prior to calcination. After drying the catalyst in the rotary evaporator, the catalyst was calcined at 673 K for 4 h. BET surface area and pore radius measurements are reported in Table 1 for the support and catalysts.

2.2. Characterization

2.2.1. Temperature programmed reduction. Temperature programmed reduction (TPR) profiles of calcined catalysts were recorded using a Zeton-Altamira AMI-200 unit which employs a thermal conductivity detector (TCD). Calcined samples were first purged at 623 K in flowing argon to remove traces of water. TPR was performed using a 10%H_2/Ar mixture and referenced to argon at a flow rate of 30 $cm^3\ min^{-1}$. The sample was heated from 323 to 1073 K using a heating ramp of 10 K min^{-1}.

2.2.2. H_2 chemisorption and percentage reduction. Hydrogen chemisorption was conducted by using temperature programmed desorption (TPD), also measured with the Zeton-Altamira AMI-200 instrument. The sample weight was 0.220 g. Catalysts were activated in a flow of 10 cm^3 of H_2 mixed with 20 cm^3 of argon at 623 K for 10 h and then cooled under flowing H_2 to 373 K. The sample was held at 373 K under flowing argon to remove and/or prevent adsorption of weakly bound species prior to increasing the temperature slowly to 623 K, the reduction temperature of the catalyst. The catalyst was held under flowing argon to desorb remaining chemisorbed hydrogen until the TCD signal returned to baseline. The TPD spectrum was integrated and the number of moles of desorbed hydrogen determined by comparing its area with the areas of calibrated hydrogen pulses. The loop volume was first determined by establishing a calibration curve with syringe injections of nitrogen in helium flow. Dispersion calculations were based on the assumption of a 1:1 H:Co stoichiometric ratio and a spherical cobalt cluster morphology.

After TPD of hydrogen, the sample was reoxidized at 623 K using pulses of oxygen. The percentage of reduction was calculated by assuming that the metal reoxidized to Co_3O_4. Further details of the procedure are provided elsewhere (Hilmen *et al.*, 1999; Jacobs, Das *et al.*, 2002).

Table 1
BET surface area (SA) and pore radius measurements for the support/catalyst.

	BET SA ($m^2\ g^{-1}$)	Average pore radius (nm)	Calcination temperature (K)
Condea Vista Catalox B γ-Al_2O_3	200	–	–
15%Co/Al_2O_3	158	4.2	673, air flow
15%Co–0.5%Pt/Al_2O_3	162	4.1	673, air flow

2.2.3. EXAFS/XANES. XAS measurements on references and catalyst samples were conducted at the National Synchrotron Light Source (NSLS) at Brookhaven National Laboratory (BNL), using beamline X18b equipped with a Si(111) channel-cut monochromator. A crystal detuning procedure was employed to prevent glitches arising from harmonics. The second crystal of the channel-cut monochromator is weakly linked to the crystal and slightly spring loaded. The other side is a picomotor, a very fine high-pitch screw that turns by piezo, which allows for slight detuning of the crystal. The X-ray ring at the NSLS has a flux of 1×10^{10} photons s^{-1} at 100 mA and 2.5 GeV, and the energy-range capability at X18b is 5.8–40 keV. The catalysts were previously activated at 673 K for 10 h in hydrogen, cooled to room temperature, purged with helium and passivated in 1% O_2 in helium for 24 h. XAFS data were recorded near the K edge of cobalt and the L_{III} edge of platinum after exposure of catalysts to flowing hydrogen at 673 K, and cooling under hydrogen flow to liquid-nitrogen temperatures. All XAFS spectra were recorded at close to the boiling temperature of nitrogen in a cell to minimize the contribution from the dynamic Debye–Waller factor.

Data reduction of the EXAFS spectra was carried out using *WinXAS* (Ressler, 1997). Standard data reduction was carried out by pre-edge background removal and normalization by division of the height of the absorption edge. XANES spectra and corresponding derivative spectra were compared after normalization. For EXAFS, χ-data were obtained by considering the single scattering region beyond 50 eV after the edge jump. Appropriate splines based on the Nyquist criteria were utilized to avoid the inclusion of excessive nodes that could destroy the data. For the case of cobalt, conversion to k space was then conducted and k weights of 0 and 3 were used, the former to allow viewing of chemical changes associated with low-Z backscatterers and the latter carried out so that examination of the changes in Co—Co coordination of the catalyst metal clusters could be ascertained after conversion to r space. Finally, the k^3-weighted results were Fourier transformed to r space to obtain the radial distribution functions. Only the k^3 weighting was used in the case of platinum.

For cobalt, fitting of the first four Co—Co coordination shells was carried out by first employing a Hanning window and then taking the back-Fourier transform. After converting to $\chi(k)$, fitting of the spectra was carried out in k space using *FEFFIT* (Newville *et al.*, 1995). The k range employed was 4–15 $Å^{-1}$. The *FEFF* program (Rehr *et al.*, 1992) was first used to construct a model of Co face-centered-cubic (f.c.c.) structure to be used in fitting, and the atomic coordinates of Co f.c.c. (with lattice parameter a = 3.544 Å) were input to the *FEFF* program with the aid of the program *ATOMS* (Ravel, 2001*a*). The samples qualitatively matched f.c.c. over hexagonal-closed-packed (h.c.p.) cobalt, as was found in a previous study of reduced supported Co clusters (Barbier *et al.*, 2001; Arčon *et al.*, 2001). In order to use the coordination number as a fitting parameter, the amplitude reduction factor S_0^2 must be fixed for all scattering paths in the solid, and it was obtained by analyzing the cobalt foil and fixing coordination numbers in the *FEFFIT* input file. The value of S_0^2 was found to be 0.835 $\pm$ 0.030, which is close to the value from a

previous study (Barbier *et al.*, 2001; Arčon *et al.*, 2001), and close to the zeroth-order approximation of 0.9 which is often utilized (Ravel, 2001*b*). Fractional coordination (n_i) for each shell, multiplying by the retained f.c.c. coordination numbers, were then varied as fitting parameters in the *FEFFIT* input file, while S_0^2 was fixed. Other fitting parameters used by *FEFFIT* included the overall E_0 shift, e_0, applied to each path and an isotropic expansion coefficient, α, which is multiplied by the nominal length of each path. Furthermore, to approximate the mean square disorder in the path length of each path, a correlated Debye model was used (Ravel, 2001*b*), with Debye temperature, θ_D, as a fitting parameter with temperature being fixed. Samples were measured at the boiling-point temperature of liquid nitrogen, which was incorporated as the temp set variable.

2.3. XPS and *in situ* reduction

Samples of Co/Al_2O_3 with and without Pt promotion were evaluated by XPS before and after *in situ* treatment with hydrogen in a high-pressure gas cell. The XPS analysis was accomplished using the $K\alpha$ line from aluminium (1486.6 eV) and an analyzer pass energy of 50 meV. Pressed powders of promoted and unpromoted samples were first analyzed by XPS at room temperature prior to any gas-phase treatment. Then the samples were exposed to $\sim 1 \times 10^6$ Pa hydrogen gas at 473, 573, 673, 773 and 873 K for 1 h with XPS analysis after each temperature step. The binding-energy shifts in the photoelectron spectrum are compared with standard spectra of $CoAl_2O_4$ and Co_3O_4. In metallic cobalt, the primary photoelectron peaks are from the $2p_{3/2}$ and $2p_{1/2}$ lines which occur at binding energies of 778 and 793 eV, respectively, with that of $2p_{3/2}$ being largest. The *in situ* sequential treatment with hydrogen allows the dynamic reduction of cobalt oxide to be monitored directly.

2.4. Catalyst testing

The calcined catalyst (*ca* 20 g) was reduced *ex situ* in a fixed-bed reactor with a mixture of hydrogen and helium (1:2) at a flow rate of 70 standard liters per hour (SL h^{-1}) at 623 K. The reactor temperature was increased from room temperature to 373 K at a rate of 2 K min^{-1} and held at 373 K for 1 h, then the temperature was increased to 623 K at a rate of 1 K min^{-1} and kept at 623 K for 10 h. The catalyst was transferred to a continuously stirred tank reactor (CSTR) to mix with 300 g of melted Polywax-3000 (polyethylene fraction with average molecular weight of 3000 g $gmol^{-1}$). To accomplish the transfer, the fixed-bed reactor was attached to the CSTR through a ball valve connection, the reduction vessel overpressured with argon, and the catalyst powder then forced through the ball valve. The reduction vessel was weighed before and after catalyst transfer to ensure that all the catalyst was added to the CSTR. The catalyst was then reduced *in situ* in the CSTR in a flow of 30 SL h^{-1} hydrogen at atmospheric pressure. The reactor temperature was increased to 503 K at a rate of 1 K min^{-1} and maintained at this activation condition for 24 h.

A 1 L CSTR was used for the slurry FTS reaction. Separate mass flow controllers were used to add hydrogen, carbon monoxide and inert gas at a desired rate to a mixing vessel. Carbon monoxide passed through a vessel containing lead-oxide–alumina to remove iron carbonyls. The mixed gases entered through a dip tube to the bottom of the CSTR. The CSTR was operated at 750 r.p.m. After the activation period the reactor temperature was decreased to 453 K, synthesis gas (H_2:CO = 2:1 to mimic ratio typical of GTL) was introduced at a space velocity of 5 SL syngas per gram of catalyst per hour and the reactor pressure was increased to 19.7 atm (2.0 MPa). The reactor temperature was then increased to 503 K at a rate of 1 K min^{-1}.

3. Results and discussion

As discussed previously, the goal of this work is to further define the role of the noble metal promoter in FTS systems by focusing on the chemistry of the Pt interaction with cobalt. In previous work (Jacobs, Das *et al.*, 2002) we obtained improved catalytic activity with the addition of 0.5% Pt to the $15\%Co/Al_2O_3$ catalyst. This improved activity was evidenced in CSTR testing as an increase in carbon monoxide conversion from 22.7% for an unpromoted system to 40.2% for the platinum-promoted catalyst.

The spinel phase of Co_3O_4 was detected by XRD in the calcined catalyst (Jacobs *et al.*, 2001). A broad TPR profile, typical of FTS cobalt catalysts, is presented in Fig. 1 for both the promoted and unpromoted samples. Two main peaks are seen for the profile of the unpromoted catalyst at the bottom of Fig. 1. The first peak at 623 K represents the conversion of Co_3O_4 to CoO, and the second peak centered near 873 K represents the further reduction of CoO to Co metal. The second reduction peak contains a shoulder near 973 K. The addition of 0.5% Pt causes both peaks to shift to lower temperatures, 498 and 773 K, and it causes both peaks to become much narrower with the loss of the higher-temperature shoulder. However, the higher-temperature peak in the upper portion of Fig. 1 is still broad. We have argued previously that the high-temperature transition of CoO to cobalt metal is incomplete owing to the interaction of cobalt species with the alumina support (Jacobs, Das *et al.*, 2002). These cluster-support interactions can account for the broadened TPR features, and while Pt addition lessens this effect it does not eliminate it. Therefore, in order to estimate the cluster size with any accuracy through chemisorption methods, it is first necessary to quantify the degree to which the cobalt has been reduced (Jacobs, Das *et al.*, 2002; Vada *et al.*, 1995). This was done by performing pulse reoxidation on the catalysts immediately after the TPD analysis. The details of the TPD analysis are presented in Table 2 for the two catalyst types. Chemisorption of hydrogen following reduction by hydrogen at 623 K for 10 h at atmospheric pressure was used to obtain the number of Co^0 surface atoms. The following equations are used to estimate cluster size:

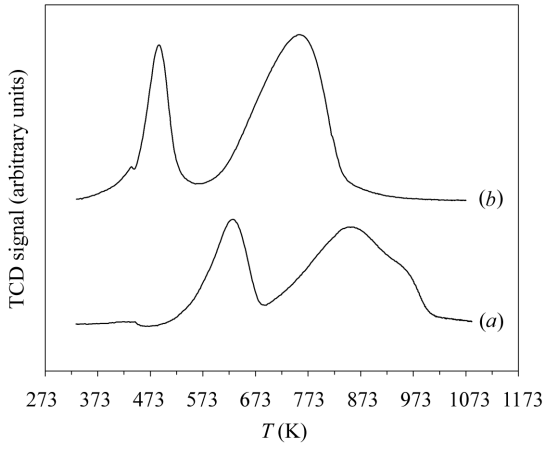

Figure 1
TPR profiles of (*a*) the unpromoted $15\%Co/Al_2O_3$ catalyst and (*b*) the $0.5\%Pt–15\%Co/Al_2O_3$ catalyst.

Table 2
Hydrogen chemisorption (TPD) and percentage reduction from pulse reoxidation.

	Reduction temperature (K)	H_2 desorbed (μmol g_{cat}^{-1})	Uncorrected %D	Uncorrected average diameter (nm)	O_2 uptake (μmol g_{cat}^{-1})	% Reduction	Corrected %D	Corrected average diameter (nm)
15%Co/Al_2O_3	623	66.9	5.3	19.6	509	30	17.5	5.9
0.5%Pt–15%Co/Al_2O_3	623	140.6	11.0	9.3	1024	60	18.4	5.6

$\%D_{uncorrected}$ = (number of Co^0 atoms on surface × 100)/(total Co^0 atoms),

$\%D_{corrected}$ = (number of Co^0 atoms on surface × 100)/[(total Co atoms in samples)(fraction reduced)].

By utilizing the correction above (note in Table 2 the error when uncorrected), the average cobalt cluster diameters for the 15%Co/Al_2O_3 catalysts were found to be close to 5.9 and 5.6 nm for unpromoted and promoted samples, respectively, almost the same within experimental error. Yet the degree of reduction was found to be much higher, 30–60%, for the promoted sample, consistent with the temperature shifts observed in TPR. Likewise, the active site density for the promoted sample was found to be approximately twofold higher, with an increase in chemisorbed hydrogen from 67 to 141 μmol g^{-1}.

Two XPS reference spectra for cobalt aluminate and cobalt oxide are reproduced in Fig. 2 (Jacobs *et al.*, 2004).

The unit cell of Co_3O_4 contains two +3 Co atoms with octahedral coordination and one atom with tetrahedral coordination in a +2 oxidation state. The $2p_{3/2}$ photoelectrons from these two cobalt oxidation states have slightly different binding energies with Co^{2+} at 780.3 eV and Co^{3+} at 779.5 eV (Hilmen *et al.*, 1999; Sexton *et al.*, 1986). The photoelectron contribution from the two oxidation states results in an asymmetric line-shape for the Co $2p_{3/2}$ peak. For cobalt aluminate, on the other hand, the Co atoms are in a +2 oxidation with tetrahedral coordination only. Cobalt aluminate has a spinel structure like cobalt oxide, but the Al atoms adopt the octahedral coordination sites in that case. Thus for $CoAl_2O_4$ the Co $2p_{3/2}$ line is more symmetric, and the peak occurs at a higher binding energy of 782 eV (Hilmen *et al.*, 1999). XPS results are presented in Fig. 3 for unpromoted 15%Co/Al_2O_3 at room temperature prior to reduction and after *in situ* reduction at various sequential temperatures. Prior to reduction at room temperature, the spectrum exhibits a broad Co $2p_{3/2}$ peak maximum at 779.1 eV with some asymmetry suggesting that the bulk of cobalt is in the form of Co_3O_4.

This finding agrees with initial powder diffraction experiments and previous XANES studies (Jacobs *et al.*, 2001; Jacobs, Patterson *et al.*, 2002). For a series of catalysts calcined in air, Co_3O_4 was found to dominate until a temperature near 823 K, where a transition to the aluminate form began to occur (Jacobs *et al.*, 2003). Hydrogen treatment causes significant changes to the photoelectron spectrum in Fig. 3. At 473 K reduction there is a slight broadening of the peak, and at 573 K there is a detectable shift in the peak maximum to 779.5 eV as the profile broadens further. Note, however, that while the $2p_{3/2}$ peak broadens it also increases slightly in symmetry. These changes are due to the conversion of Co_3O_4 to CoO, where Co^{3+} atoms which produce photoelectrons at lower binding energy (779.5 eV) undergo reduction to a +2 state producing photoelectrons at a higher binding energy (780.3 eV), but the broadening is presumably caused by interactions with the support producing a partially reduced phase. Partial cobalt reduction is evident at 673 K as a splitting of the broad peak into a sharper peak at low binding energy is consistent with cobalt metal. Interestingly, the broader peak moves to higher binding energy with increasing reduction temperature. From 573 to 873 K the shift is an additional 0.7 eV, producing a peak maximum at 780.2 eV. This lends credence to the idea that a fraction of CoO which is difficult to reduce remains on the surface.

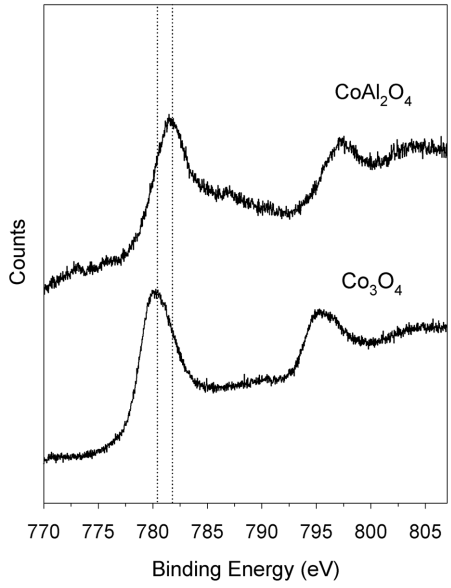

Figure 2
XPS spectra of Co_3O_4 and $CoAl_2O_4$ reference spectra. Dotted lines denote positions of peak maxima.

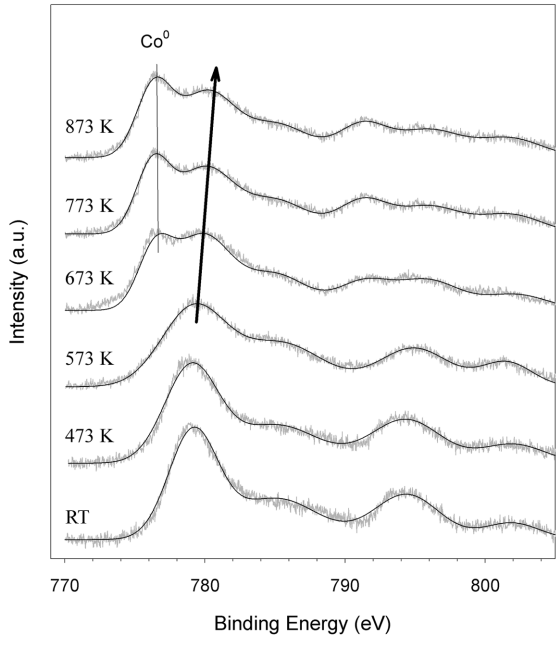

Figure 3
XPS spectra of unpromoted 15%Co/Al_2O_3 after exposure to 60 min hydrogen treatment and subsequent evacuation at, moving upward, room temperature (RT), 473 K, 573 K, 673 K, 773 K and 873 K.

Such was the observation in a previous study of a cobalt-Kieselguhr Fischer-Tropsch catalyst (Sexton *et al.*, 1986). In that report, although Co_3O_4 reduction to CoO was affected very little, the kinetics of CoO reduction were substantially hindered in the presence of oxides such as ThO_2 and MgO (Sexton *et al.*, 1986). However, in the case of Co/Al_2O_3 it is important to note that in a TPR investigation a small fraction of cobalt remained as cobalt aluminate, even at cobalt loadings of 20% and 30% (Wang & Chen, 1991). This small fraction of cobalt was found to reduce only at temperatures higher than 1073 K. In our study we did not heat the sample above 873 K, and it is very likely that a fraction of cobalt aluminate contributes to the high-energy section of the Co $2p_{3/2}$ line in the XPS in Fig. 3. However, in comparing the higher-energy $2p_{3/2}$ residual feature in Fig. 3 with the reference spectrum of $CoAl_2O_4$ in Fig. 2, it is evident that the binding energies do not match exactly, with $CoAl_2O_4$ having a peak maximum near 782 eV and the residual oxide closer to 780 eV. Therefore, the residual oxide present after reduction of unpromoted Co/Al_2O_3 contains other oxide forms in addition to cobalt aluminate.

Arnoldy & Moulijn (1985) have argued that the series of peaks in the TPR of Co/Al_2O_3 catalysts consist of several contributors. In agreement with Sexton *et al.* (1986), for a sample calcined at 623 K, they show a sharp peak at a low temperature and a broad profile with multiple peaks. The sharp peak was assigned to the reduction of bulk crystallites of Co_3O_4 to Co metal, and the broad profile was assigned to the reduction of a mixed dispersed surface interaction of cobalt and alumina support, with cobalt in the +2 and/or +3 oxidation states depending on the nature of the cobalt alumina complex (Arnoldy & Moulijn, 1985). In recent TPR work including a variety of supports, it was found in all cases that the area ratio of the first peak to that of the second was always very close to 1:3 (Jacobs *et al.*, 2001; Jacobs, Das *et al.*, 2002) which agreed with the findings of Sexton *et al.* (1986). This 1:3 ratio held true whether the peaks were sharp, as for cobalt oxide and Co/SiO_2, or broadened, as for ZrO_2-modified silica-, titania- or alumina-supported cobalt catalysts. This is consistent with the stoichiometry of cobalt oxide reduction in two steps (Co_3O_4 to CoO to Co^0), where the second higher-temperature step consumes three times as much hydrogen as the first. However, there is the possibility of solid solution formation between CoO and the support which would inhibit the kinetics of reduction. For Co/Al_2O_3 catalysts reduced at temperatures above the first peak, we found that the XANES spectra contained a CoO component which dominated the spectra (Jacobs *et al.*, 2001; Jacobs, Patterson *et al.*, 2002). Certainly, after calcination of the catalyst, the major species is Co_3O_4 (Jacobs *et al.*, 2001; Jacobs, Patterson *et al.*, 2002), but after the first stage of reduction (Co_3O_4 to CoO) it is likely that CoO exhibits a range of surface interactions that depend strongly on the support. For a series of catalysts calcined at increasing temperatures (Jacobs *et al.*, 2003), we found that the entire TPR profile also shifts to higher temperatures; however, the peak areas of the first sharp feature to the second broad profile still maintained a 1:3 ratio. Upon calcination at temperatures above 823 K, the entire TPR profile was attenuated as cobalt aluminate formed, consistent with XANES interpretation (Jacobs *et al.*, 2003). We therefore consider that the two peaks of the profile reflect a two-step reduction passing through CoO as an intermediate: $Co_3O_4 \rightarrow CoO \rightarrow Co^0$. Another study using XANES (Bart, 1986; Castner *et al.*, 1983) examined the reduction of silica-supported Co catalysts with varying cluster sizes of 5–100 nm. In that report it was argued that the strong interaction of the small particles with the support aided in stabilizing the oxide phase. That is, while a rapid Co_3O_4 to CoO reduction was reported for the 523–573 K range for all catalyst samples, the CoO to Co^0 step showed a strong dependence on cluster size and support interaction. Cobalt clusters on alumina-supported catalysts were found in our previous study to be smaller than similarly loaded SiO_2- and TiO_2-supported Co catalysts with cluster sizes below 10 nm (Jacobs, Das *et al.*, 2002). It is therefore not surprising that these supported cobalt oxide systems will deviate from the behavior of the bulk reduction of Co_3O_4. Returning to the XPS interpretation of the residual oxide present for the unpromoted system in Fig. 3, it can be conjectured that the 780 eV region reflects contributions from such unreduced CoO particles. Recall that the binding energy of this region was 2 eV lower than expected for a pure cobalt aluminate; thus, these unreduced particles with strong surface interactions may be the dominant residual cobalt oxide form in the unpromoted catalyst materials.

Platinum addition to the Co/Al_2O_3 catalyst has significant effects on the activation of this material. The XPS of cobalt/alumina with 0.5% Pt promotion is presented in Fig. 4 for an unreduced room-temperature sample and a sample which has been reduced at sequentially higher temperatures. The treatment was identical to that for the unpromoted catalyst, yet there are significant differences in behavior. The reduction to cobalt metal is more pronounced at a lower temperature of 573 K, and the extent of reduction to a metallic state is much greater upon treatment at 873 K than for the unpromoted catalyst. From the TPR analysis, a complete reduction of CoO to Co^0 only occurs upwards of 1123 K. It is anticipated from experience and observed in the XPS in Fig. 4 that a fraction of cobalt species should remain in the unreduced state. Notwithstanding, it is evident that the residual XPS peak is both significantly lower in intensity and higher in binding energy than in the previous case of the unpromoted catalyst. The residual peak at 782 eV does indeed match the assignment of cobalt aluminate when compared with the spectrum in Fig. 2. This observation in the XPS also supports the argument that the small feature present in TPR (discussed earlier) be interpreted as residual cobalt aluminate (Wang & Chen, 1991). In Table 3 the percent reduction of cobalt oxides is presented as a function of thermal treatment, and the percent reduction is taken as

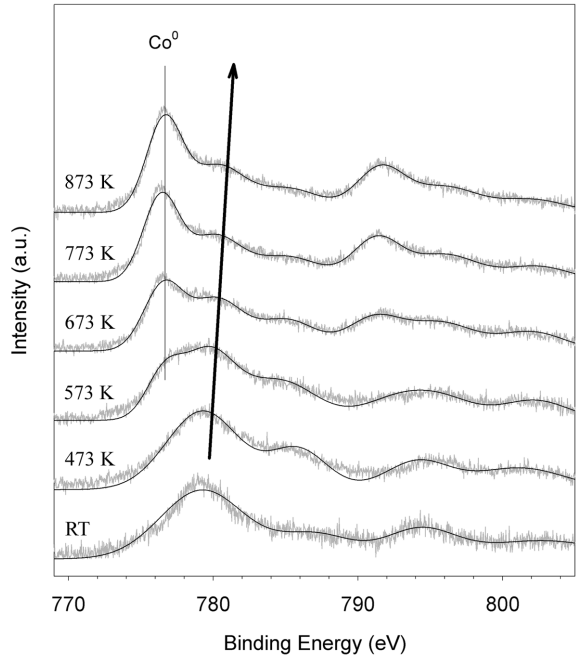

Figure 4
XPS spectra of 0.5%Pt-promoted 15%Co/Al_2O_3 after exposure to 60 min hydrogen treatment and subsequent evacuation at, moving upward, room temperature, 473 K, 573 K, 673 K, 773 K and 873 K.

Table 3
Percentage reduction by ratio of metal to oxide calculated using XPS data.

	15%Co/Al_2O_3	0.5%Pt–15%Co/Al_2O_3
Sample reduced at:		
473 K	0%	0%
573 K	0%	31%
673 K	31%	49%
773 K	37%	57%
873 K	41%	59%

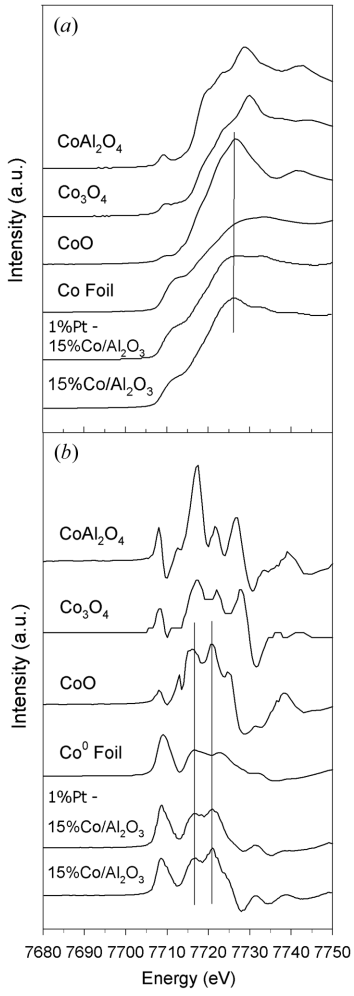

Figure 5
(*a*) XANES normalized spectra. Catalysts reduced at 673 K *in situ* with hydrogen and cooled under hydrogen. All samples cooled to liquid-nitrogen temperature prior to scanning. (*b*) XANES derivative spectra.

the area ratio of the metal Co $2p_{3/2}$ line to that of the residual line. It is clearly shown in Table 3 that Pt addition increases both the extent and efficiency of cobalt reduction.

In Fig. 5 XANES spectra in direct and derivative intensity mode are reported for both promoted and unpromoted sample types after *in situ* reduction (45 min for the reduced/passivated sample), and spectra are also provided for four reference types: Co^0, Co_3O_4, CoO and $CoAl_2O_4$. Platinum addition is also observed to increase the extent of cobalt reduction. This is seen in XANES as an increase in the 7712 eV shoulder relative to the higher-energy spectrum, more perceptible in the derivative spectrum. For the unpromoted catalyst the main residual oxide component contributing to the XANES is CoO rather than $CoAl_2O_4$ as seen by the sharp peak at 7726 eV in

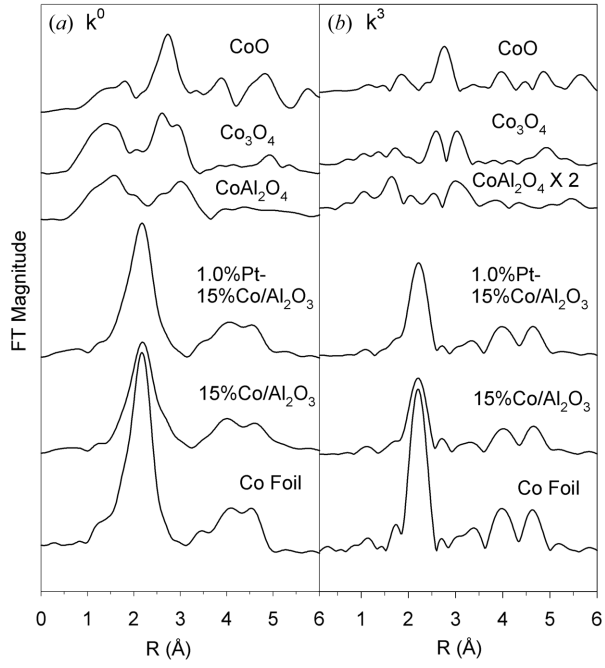

Figure 6
(*a*) k^0- and (*b*) k^3-weighted Fourier transform magnitude spectra. Catalysts reduced at 673 K *in situ* with hydrogen and cooled under hydrogen. All samples were cooled to liquid-nitrogen temperature prior to scanning.

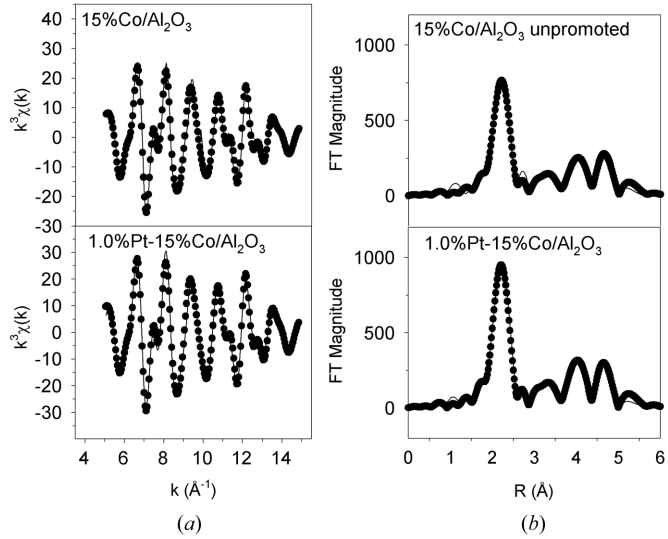

Figure 7
(*a*) k^3-weighted $\chi(k)$ *versus* k and (*b*) k^3-weighted Fourier transform magnitude spectra. Solid lines indicate the experimental data, while the dotted points show the results of fitting with *FEFFIT*. Catalysts reduced at 673 K *in situ* with hydrogen and cooled under hydrogen prior to scanning.

Fig. 5(*a*). The dominance of CoO in the unsupported catalyst was anticipated from the previous XPS discussion and is due to small oxide clusters interacting strongly with the support. While the Pt-promoted catalyst has a greater extent of reduction, there are still contributions from CoO inasmuch as aluminate contributions are harder to distinguish in XANES.

Looking at the Co *K*-edge in EXAFS can provide insight into the type of interatomic bonds present in the sample. These EXAFS of both k^0- and k^3-weighted data are presented in Fig. 6 for promoted and unpromoted samples and for the reference materials, and in Fig. 7

Table 4
Effect of platinum reduction promotion on the fractional coordination (n_i) of Co neighbor atoms in the first four coordination shells of cobalt clusters supported on Al_2O_3.

n_1, fractional coordination in ith shell; e_0, phase correction parameter (overall E_0 shift applied to each path in eV); α, isotropic expansion coefficient; T_D, Debye temperature; R factor, fractional misfit.

	n_1	Δn_1	n_2	Δn_2	n_3	Δn_3	n_4	Δn_4	e_0	Δe_0	α	$\Delta\alpha$	T_D (K)	ΔT_D (K)	R factor
Cobalt K edge															
15%Co/Al_2O_3	0.70	0.05	0.66	0.08	0.52	0.06	0.44	0.06	7.30	0.81	−0.0030	0.0017	318	29	0.0187
1%Pt–15%Co/Al_2O_3	0.76	0.06	0.69	0.07	0.60	0.05	0.46	0.06	7.00	0.85	−0.0042	0.0018	330	37	0.0194
Cobalt metal f.c.c.	12		6		24		12								

the k^3 Fourier transform is plotted against k space for the two catalysts. The dominant contribution comes from cobalt metal as evidenced by the similarity of the spectra in Fig. 6 to cobalt metal foil at 2, 4 and 4.5 Å and the almost identical structure of the transforms in Fig. 7. Such similarity has been observed in other EXAFS investigations of cobalt alumina FTS catalysts (Jacobs *et al.*, 2001; Jacobs, Patterson *et al.*, 2002). Only a small shoulder in the k^0-weighted and a very small peak in the k^3-weighted spectra are observed at a distance of 2.6 Å for Co—Co coordination in the CoO oxide for the unpromoted and promoted catalyst samples, although evidence of significant CoO contribution was detected in XANES and XPS results. The low magnitude of the 2.6 Å feature as compared with bulk CoO may also reflect strong substrate interactions in the promoted catalyst as well as in the unpromoted sample.

Fitting using *FEFFIT* in k space and a correlated Debye model (Fig. 7) was used to elucidate differences in cobalt cluster size between the unpromoted and promoted catalysts. Good fits were obtained, as indicated by the R factor, which is less than 0.02 in each case. A comparison of Figs. 6 and 7 shows that the Pt-promoted catalyst contains slightly larger cobalt clusters than the unpromoted sample. However, these clusters were found to be similar in size by chemisorption and pulse reoxidation (Table 2). In Table 4 a comparison of the EXAFS data is made with the average neighbor fractions of f.c.c. magic number clusters (Barbier *et al.*, 2001; Arčon *et al.*, 2001), and the comparison indicates that the clusters are between 1 nm and 2 nm in size. This cluster size is significantly smaller than the average value given by hydrogen chemisorption (Table 2) and XRD, which both give estimates between 5 nm and 10 nm (Jacobs *et al.*, 2001, 2004; Jacobs, Das *et al.*, 2002). In similar EXAFS studies using Co/silica FTS catalysts, cluster sizes were found to be smaller than those obtained through magnetic measurements and microscopy (Barbier *et al.*, 2001; Arčon *et al.*, 2001). Furthermore, the EXAFS is far more sensitive to metallic cobalt moieties as can be seen in the relative magnitude of the spectra in Fig. 6. While XANES clearly identifies that a fraction of cobalt remains in an unreduced state after the reduction procedure, peaks for Co—O bonding are not evident in the FT magnitude spectra. Therefore, to emphasize Co—Co coordination and de-emphasize coordination to low-Z backscatterers, χ spectra were k^3 weighted, and the Hanning window employed over the first four Co—Co coordination shells. There are also limitations on determining cobalt cluster size by chemisorption methods. Certainly the temperature at which the chemisorption is conducted influences the surface coverage, and can result in overestimation (if T is too high), or, conversely, an underestimation (if T is too low). Likewise, there is also a degree of error in the extent of reduction measurements obtained from pulse reoxidation.

Even considering the degree of error associated with each technique the difference between the two average cluster sizes is still quite large (*i.e.* difference between 2 nm by EXAFS and 6 nm by chemisorption results in a factor of ten in surface area). We consider three possibilities that could account for the discrepancy. First of all, the morphology may not be spherical. The first four shells were fitted and the relative fractional coordination numbers are consistent with a spherical cluster. However, a heterogeneity in structure could conceivably average out to give the appearance of a spherical cluster.

There are two more likely explanations, however. It is important to reconsider what each technique is measuring. Chemisorption techniques assume that the surface atoms are exposed to the gas phase. With Co/Al_2O_3, however, where there are strong interactions with the support [*i.e.* the strong metal support interactions (SMSI)], this may not be the case. As displayed in Fig. 8(*a*), since not all of the surface Co atoms are available to the gas phase, the SMSI effect can lead to overestimates of the average crystallite size. A similar effect is observed when the metal crystallites are aggregated on the support surface, as shown in Fig. 8(*b*). In that case, cobalt domains within an aggregate may not be exposed to the gas phase, leading again to an overestimate of the average cluster size by chemisorption (Arčon *et al.*, 2001).

For both situations, in the case of hydrogen chemisorption the number of hydrogen molecules adsorbed will be less than that of the ideal cluster model, where all Co crystallite atoms on the surface are assumed to be exposed to the gas phase.

The Fourier transform magnitude at the L_{III} edge is given for pure Pt metal and the Pt-loaded catalyst in Fig. 9, and the k^3 $\chi(k)$ correlation in k space is presented in Fig. 10 for the same samples. The

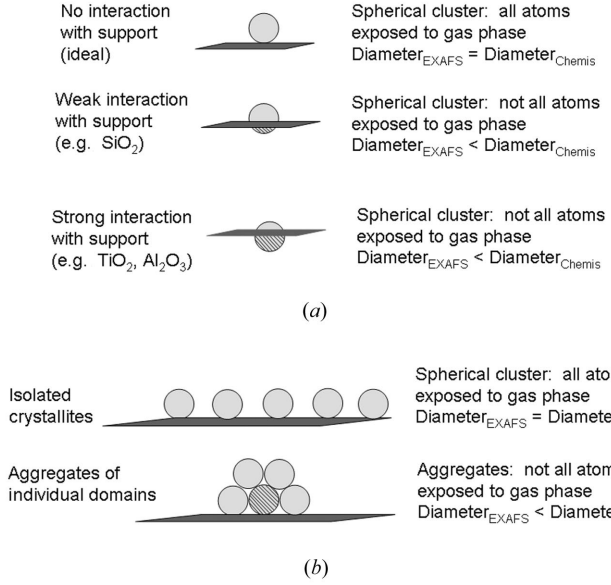

Figure 8
(*a*) Influence of the metal support interaction. (*b*) Influence of crystallite aggregation.

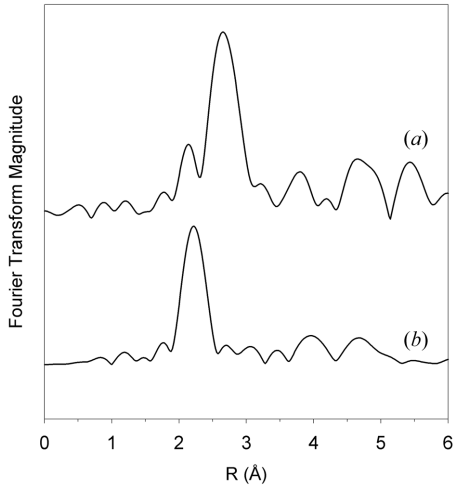

Figure 9
(*a*) Pt foil and (*b*) reduced 1%Pt–15%Co/Al_2O_3 catalyst k^3-weighted Fourier transform magnitude spectra. Catalyst reduced at 673 K *in situ* with hydrogen and cooled under hydrogen.

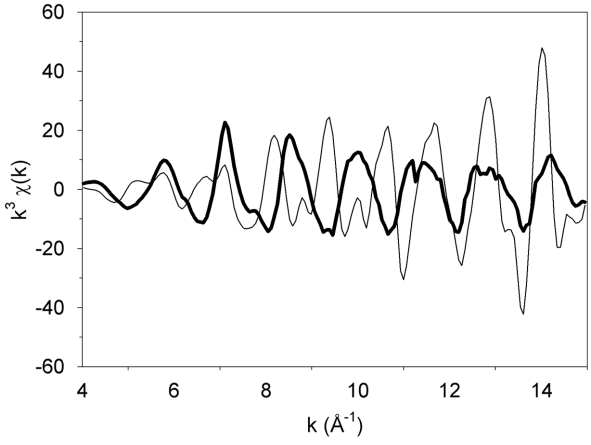

Figure 10
Pt foil (light line) and reduced 1%Pt–15%Co/Al_2O_3 catalyst (dark line) k^3-weighted $\chi(k)$ spectra. Catalyst reduced at 673 K *in situ* with hydrogen and cooled under hydrogen.

catalyst showed a distinct peak at about 2.1 Å which is ~0.6 Å contracted from the first coordination shell of Pt metal. The size of the peak for the catalyst is likely to rule out a Pt—Pt contracted bond distance which is only observed for very small Pt clusters. Such is the case for Pt clusters supported on microporous zeolite where the FT magnitude is substantially attenuated (Jacobs *et al.*, 2000). Furthermore, Fig. 11 shows that the Pt promoter in the catalyst is in the reduced state (the white line for the catalyst is even smaller than that of the Pt metal foil). As shown in Fig. 11, and as expected, the white line for Pt oxide (also shown) is much more intense than even that of the Pt foil. Therefore the peak in the FT magnitude does not correspond to Pt—O coordination. Rather, the results indicate that Pt is not coordinated to Pt metal or oxygen but rather to cobalt, as previously reported by Guczi *et al.* (2002). An inspection of the higher coordination shells with that of cobalt metal at 4 Å and 4.7 Å gives credibility to this assignment. The *k*-space correlation in Fig. 10 reveals that the Pt contribution from the catalyst is distinctly out of phase with that of the foil. This further indicates that Pt is present as atoms isolated from other Pt atoms but in intimate contact with

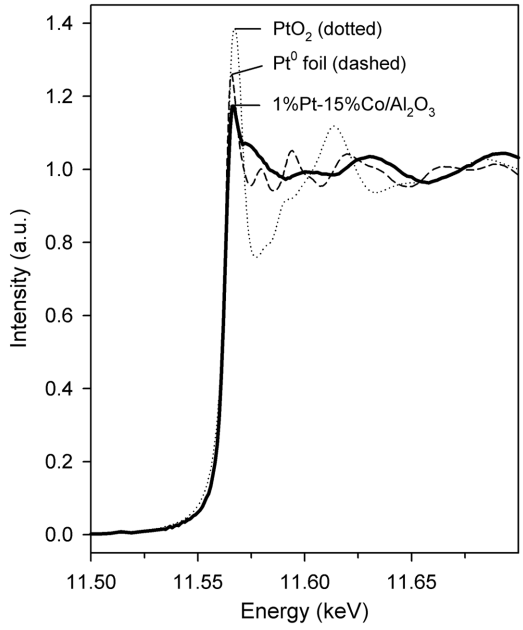

Figure 11
XANES normalized spectra at the Pt L_{III} edge.

cobalt clusters. Without additional evidence it is difficult to determine whether the Pt atoms are located on the surface of the cobalt or within the cluster itself as an alloy. As suggested in the introduction, hydrogen spill-over from the noble metal may be the means by which platinum assists in cobalt reduction. On this basis, Pt would need to be located on the Co cluster in a position in contact with the gas phase and not solely constrained to the interior.

4. Conclusions

Upon calcination of both unpromoted and Pt-promoted Co/Al_2O_3 catalysts the mixed-oxidation-state oxide, Co_3O_4, is the dominant form of cobalt present. The transition of Co_3O_4 to CoO occurs readily at 623 K and 523 K for the unpromoted and promoted systems, respectively, as seen in TPR. The second reduction of CoO to Co is the important step in creating catalytically active sites, but this second step is cluster-size dependent and hindered by the interaction of CoO with the alumina support. The interaction of cobalt oxides with the underlying support results in broad TPR profiles for the second stage of reduction and the creation of residual oxides which are difficult to completely reduce. Analysis of the residual oxides with XPS and XANES shows that they consist of CoO bound to the support and Co bound to the support as an aluminate. Platinum addition to the catalyst decreases the temperature of both reduction steps and increases the ultimate amount of cobalt metal formed in the process while creating catalyst clusters of similar size to that of the unpromoted system. For a standard reduction temperature of 623 K, platinum decreases the amount of CoO bound to the support, but a small amount of irreducible $CoAl_2O_4$ remains as evidenced by XPS and corroborated by TPR. Platinum is dispersed in the catalyst with no evidence from EXAFS for the formation of Pt—Pt bonds. These platinum atoms must be in intimate contact with the cobalt cluster to account for a spill-over mechanism and the observed Fourier transform of the coordination shells.

This work was supported by US DOE contract number DE-AC22-94PC94055 and the Commonwealth of Kentucky. This research was

carried out, in part, at the National Synchrotron Light Source, Brookhaven National Laboratory, which is supported by the US DOE, Divisions of Materials Science and Chemical Sciences. Special thanks to Dr Syed Khalid (beamline X18b, NSLS, Brookhaven) for help with the XAFS studies, and Joel Young (University of Oklahoma, Department of Physics) for XAFS cell construction.

References

Arčon, I., Tuel, A., Kodre, A., Martin, G. & Barbier, A. (2001). *J. Synchrotron Rad.* **8**, 575–577.
Arnoldy, P. & Moulijn, J. A. (1985). *J. Catal.* **93**, 38–54.
Barbier, A., Tuel, A., Arcon, I., Kodre, A. & Martin, G. A. (2001). *J. Catal.* **200**, 106–116.
Bart, J. (1986). *Adv. Catal.* **34**, 203–296.
Bechara, R., Balloy, D., Dauphin, J-Y. & Grimblot, J. (2002). *Chem. Mater.* **11**, 1703–1711.
Berge, P. J. van, Barradas, S., van de Loosdrecht, J. & Visagie, J. L. (2001). *Erdol Erdgas Kohle*, **117**, 138–142.
Castner, D. G., Watson, P. R. & Dimpfl, W. L. (1983). SSRL Activity Report Proposal No. 628M, P. VII-57. SSRL, Stanford, CA, USA.
Enache, D. I., Rebours, B., Roy-Auberger, M. & Revel, R. (2002). *J. Catal.* **205**, 346–353.
Espinoza, R. L., Visagie, J. L., van Berge, P. J. & Bolder, F. H. (1998). US Patent 5 733 839.
Guczi, L., Bazin, D., Kovacs, I., Borko, L., Schay, Z., Lynch, J., Parent, P., Lafon, C., Stefler, G., Koppany, Z. & Sajo, I. (2002). *Top. Catal.* **20**, 129–139.
Hilmen, A. M., Schanke, D., Hanssen, K. F. & Holmen, A. (1999). *Appl. Catal. A*, **186**, 169–188.
Hilmen, A. M., Schanke, D. & Holmen, A. (1996). *Catal. Lett.* **38**, 143–147.
Jacobs, G., Chaney, J. A., Patterson, P. M., Das, T. K. & Davis, B. H. (2004). *Appl. Catal. A*, **264**, 203–212.
Jacobs, G., Das, T. K., Patterson, P. M., Li, J., Sanchez, L. & Davis, B. H. (2003). *Appl. Catal. A*, **247**, 335–343.
Jacobs, G., Das, T. K., Zhang, Y., Li, J., Racoillet, G. & Davis, B. H. (2002). *Appl. Catal. A*, **233**, 263–281.
Jacobs, G., Ghadiali, G., Pisanu, F., Pisanu, C. L., Borgna, A., Alvarez, W. E. & Resasco, D. E. (2000). *J. Catal.* **191**, 116–127.
Jacobs, G., Patterson, P. M., Das, T. K., Luo, M. & Davis, B. H. (2004). *Appl. Catal. A*. In the press.
Jacobs, G., Patterson, P. M., Zhang, Y., Das, T. K., Li, J. & Davis, B. H. (2002). *Appl. Catal. A*, **233**, 215–226.
Jacobs, G., Zhang, Y., Das, T. K., Li, J., Patterson, P. M. & Davis, B. H. (2001). *Stud. Surf. Sci. Catal.* **139**, 415–422.
Jongsomjit, B., Panpranot, J. & Goodwin, J. G. Jr (2001). *J. Catal.* **204**, 98–109.
Kogelbauer, A., Goodwin, J. G. Jr & Oukaci, R. (1996). *J. Catal.* **160**, 125–133.
Lapidus, A., Krylova, A., Kazanskii, V., Borovkov, V., Zaitsev, A., Rathousky, J., Zukal, A. & Jancalkova, M. (1991). *Appl. Catal.* **73**, 65–82.
Loosdrecht, J. van de, Barradas, S., Caricato, E. A., van Berge, P. J. & Visagie, J. L. (2000). *Am. Chem. Soc. Div. Fuel Chem. Prepr.* **45**, 587–591.
Moen, A. & Nicholson, D. G. (1997). *Chem. Mater.* **9**, 1241–1247.
Newville, M., Ravel, B., Haskel, D., Stern, E. A. & Yacoby, Y. (1995). *Physica B*, **208**/**209**, 154–156.
Ravel, B. (2001*a*). *J. Synchrotron Rad.* **8**, 314–316.
Ravel, B. (2001*b*). *EXAFS Analysis Using FEFF and FEFFIT Workshop*, 27–29 June 2001. NSLS, Brookhaven National Laboratory, Upton, NY, USA.
Rehr, J. J., Zabinsky, S. I. & Albers, R. C. (1992). *Phys. Rev. Lett.* **69**, 3397–3400.
Ressler, T. (1997). *WinXAS97.* Version 1.0. [http://www.winxas.de.]
Ronning, M., Nicholson, D. G. & Holmen, A. (2001). *Catal. Lett.* **72**, 141–146.
Rygh, L. E. S. & Nielsen, C. J. (2000). *J. Catal.* **194**, 401–409.
Schanke, D., Vada, S., Blekkan, E. A., Hilmen, A. M., Hoff, A. & Holmen, A. (1995). *J. Catal.* **156**, 85–95.
Sexton, B. A., Hughes, A. E. & Turney, T. W. (1986). *J. Catal.* **97**, 390–406.
Tang, S., Lin, J. & Tan, K. L. (1999). *Surf. Interf. Anal.* **28**, 155–158.
Vada, S., Hoff, A., Adnanes, E., Schanke, D. & Holmen, A. (1995). *Top. Catal.* **2**, 155–162.
Voss, M., Borgmann, D. & Wedler, G. (2002). *J. Catal.* **212**, 10–21.
Wang, W-J. & Chen, Y.-W. (1991). *Appl. Catal.* **77**, 223–233.